



RESEARCH LETTER

10.1002/2017GL076630

Key Points:

- Solar-induced fluorescence explains regional net ecosystem exchange over North America better than existing data sets and mechanistic models
- Information provided by SIF is particularly beneficial for explaining the NEE signal in croplands and needleleaf forests
- SIF-informed inverse estimates of NEE sinks show consistent growing season shift from needleleaf forests to croplands in North America

Supporting Information:

- Supporting Information S1

Correspondence to:

Y. P. Shiga,
yshiga@stanford.edu

Citation:

Shiga, Y. P., Tadić, J. M., Qiu, X., Yadav, V., Andrews, A. E., Berry, J. A., & Michalak, A. M. (2018). Atmospheric CO₂ observations reveal strong correlation between regional net biospheric carbon uptake and solar-induced chlorophyll fluorescence. *Geophysical Research Letters*, 45, 1122–1132. <https://doi.org/10.1002/2017GL076630>

Received 23 AUG 2017

Accepted 12 DEC 2017

Accepted article online 19 DEC 2017

Published online 24 JAN 2018

Atmospheric CO₂ Observations Reveal Strong Correlation Between Regional Net Biospheric Carbon Uptake and Solar-Induced Chlorophyll Fluorescence

Yoichi P. Shiga^{1,2} , Jovan M. Tadić^{1,3} , Xuemei Qiu¹, Vineet Yadav⁴ , Arlyn E. Andrews⁵ , Joseph A. Berry¹, and Anna M. Michalak¹ 

¹Department of Global Ecology, Carnegie Institution for Science, Stanford, CA, USA, ²Department of Civil and Environmental Engineering, Stanford University, Stanford, CA, USA, ³Now at Climate and Ecosystem Sciences Division, Lawrence Berkeley National Lab, Berkeley, CA, USA, ⁴Science Data Understanding Group, Jet Propulsion Laboratory, Pasadena, CA, USA, ⁵Earth System Research Laboratory, National Oceanic and Atmospheric Administration, Boulder, CO, USA

Abstract Recent studies have shown the promise of remotely sensed solar-induced chlorophyll fluorescence (SIF) in informing terrestrial carbon exchange, but analyses have been limited to either plot level (~1 km²) or hemispheric/global (~10⁸ km²) scales due to the lack of a direct measure of carbon exchange at intermediate scales. Here we use a network of atmospheric CO₂ observations over North America to explore the value of SIF for informing net ecosystem exchange (NEE) at regional scales. We find that SIF explains space-time NEE patterns at regional (~100 km²) scales better than a variety of other vegetation and climate indicators. We further show that incorporating SIF into an atmospheric inversion leads to a spatial redistribution of NEE estimates over North America, with more uptake attributed to agricultural regions and less to needleleaf forests. Our results highlight the synergy of ground-based and spaceborne carbon cycle observations.

1. Introduction

The terrestrial biosphere currently absorbs approximately one quarter of anthropogenic carbon dioxide emissions resulting from fossil fuel burning (Le Quéré et al., 2016). However, estimates of the present and future magnitude, seasonality, and spatiotemporal patterns of these terrestrial carbon fluxes remain highly uncertain (Fang et al., 2014; Friedlingstein et al., 2014; Sitch et al., 2008). Global maps of remotely sensed solar-induced chlorophyll fluorescence (SIF), an emission that originates from the photosynthetic machinery of plants, offer the potential to directly track changes in photosynthetic activity and thus carbon uptake across a variety of spatiotemporal scales (Frankenberg et al., 2011; Guanter et al., 2014; Joiner et al., 2014; Magnani et al., 2014). While the exact nature of the mechanistic relationship between SIF and gross primary production (GPP) is still uncertain and warrants further study (Porcar-Castell et al., 2014; van der Tol et al., 2009), an empirical relationship has been observed between satellite-based observations of SIF and estimates of GPP from flux towers and biospheric models (Frankenberg et al., 2011; Guanter et al., 2014; Joiner et al., 2014; Yang et al., 2015). The empirical GPP-SIF relationship, while promising, relies primarily on plot-scale (~1 km²) GPP estimates. A logical next step in the exploration of the utility of SIF as a carbon cycle data set is to examine the efficacy of SIF measurements to constrain surface carbon fluxes at critical intermediate (e.g., biome/regional) scales.

Observations of atmospheric CO₂ concentrations (hereafter “atmospheric observations”) provide an opportunity to investigate SIF at important yet difficult to explore regional scales (e.g., Parazoo et al., 2013). Atmospheric observations have long provided a diagnostic to monitor the carbon cycle at global scales by tracking the rise and fall of CO₂ concentrations (Keeling et al., 1976; Tans et al., 1990). While individual tower-based atmospheric observations may integrate the influence of large areas (up to ~10⁶ km²) (Gloor et al., 2001), relatively dense networks of atmospheric observations (e.g., over North America) have enabled investigations into regional-scale patterns of net ecosystem exchange (NEE) (Göckede et al., 2010; Lauvaux et al., 2012; Schuh et al., 2013). Furthermore, networks of atmospheric observations have been shown to provide an intermediate-scale constraint not only for NEE but also for relationships between NEE and enviro-climatic variables that explain the spatiotemporal variability of NEE (Fang & Michalak, 2015; Gourdji et al., 2012).

Here we use a network of atmospheric observations over North America to compare the ability of SIF and other surface-level enviro-climatic or vegetative variables (e.g., temperature, precipitation, and other vegetation indices; hereafter “explanatory variables”) to explain the space–time patterns of NEE. We use an atmospheric transport model (hereafter “transport model”) to relate the space–time patterns of the explanatory variables to fluctuations in atmospheric observations from a network of towers across North America. Second, we compare two sets of inverse-modeling-derived estimates of NEE, one set that incorporates SIF into the inversion and another set that relies only on other existing explanatory variables. In this way, we assess how SIF (by tracking GPP) impacts the space–time patterns of inverse estimates of NEE.

2. Data

2.1. Atmospheric CO₂ Data

We use ~23,000 three-hourly average atmospheric observations from North American continuous in situ CO₂ measurement sites over 3 years, 2008–2010. Most data are sourced from the ObsPack product: GLOBALVIEWplus v2.1 (ObsPack GLOBALVIEWplus v2.1, 2016) with the exception of sites supported by the Mid-Continent Intensive project (Miles et al., 2012, 2013) located in Austin Cary Memorial Forest, Gainesville, Florida (AAC); Chestnut Ridge, Tennessee (ACR); Canaan Valley, West Virginia (ACV); Mead, Nebraska (AME); Missouri Ozark, Missouri (AOZ) (Stephens et al., 2011); Centerville, Iowa (RCE); Galesville, Wisconsin (RGV); Kewanee, Illinois (RKW); Mead, Nebraska (RMM); Round Lake, Minnesota (RRL) (S. J. Richardson et al., 2012); and Rosemount, Minnesota (KCMP) (Griffis et al., 2008), as well as the site at Harvard Forest, Massachusetts (HFM) (Urbanski et al., 2007) (see Table S1 in the supporting information for tower locations, names, heights, and data providers). The atmospheric observations were filtered similar to Fang and Michalak (2015) to exclude anomalous data associated with low-quality flags, extreme outliers, large spikes of ± 30 ppm from background, and possible transport model issues. In order to focus on the biospheric signal of North America we removed the influence of fossil fuel CO₂ emissions and boundary conditions. Boundary conditions or background CO₂ values were calculated similar to Jeong et al. (2017), using a three-dimensional curtain estimated from marine boundary layer data (Cooperative Air Sampling Network—<http://www.esrl.noaa.gov/gmd/ccgg/flask.html>) and vertical profile data from aircraft (<http://www.esrl.noaa.gov/gmd/ccgg/aircraft/>). We used fossil fuel emission estimates from the fossil fuel data assimilation system scaled to a $1^\circ \times 1^\circ$ spatial scale and three-hourly temporal resolution (Asefi-Najafabady et al., 2014). For additional information regarding the atmospheric observations see the supporting information Text S1.

2.2. Explanatory Variables

We use a number of environmental data sets as possible explanatory variables for NEE. These include SIF and four other remotely sensed vegetation indices: the enhanced vegetation index (EVI), leaf area index (LAI), fraction of photosynthetically active radiation (FPAR), and the normalized difference vegetation index (NDVI) (Huete et al., 2002; Joiner et al., 2013; Tucker et al., 2005; Zhu et al., 2013), as well as variables related to water availability and temperature from the North American Regional Reanalysis (Mesinger et al., 2006) including temperature, precipitation rate, soil moisture, downwelling shortwave radiation (DSWR), snow cover, specific humidity (SpHum), and relative humidity. A detailed description of the data sets can be found in the supporting information Text S1.

All of the explanatory variables have been scaled to a $1^\circ \times 1^\circ$ spatial and 15 or 16 day temporal resolution (note that this is coarser than the three-hourly atmospheric observations). The relatively coarse temporal resolution is used to match that of the coarsest explanatory variable, in order to better isolate the relative value of the various variables in tracking NEE, rather than confound the impact of differences in temporal resolution. We use the spatiotemporal kriging approach of Tadić et al. (2017) to map SIF from the level 2 SIF data (v26) from GOME-2 (Joiner et al., 2013).

3. Methods

We use the Weather Research and Forecasting (WRF) model (Nehrkorn et al., 2010; Skamarock & Klemp, 2008) coupled with the Stochastic Time-Inverted Lagrangian Transport (STILT) model (Lin et al., 2003) as the transport model to calculate the sensitivity ($\text{ppm}/(\mu\text{mol}/\text{m}^2\text{s})$) of each atmospheric observation to upwind surface

regions, defined here at a $1^\circ \times 1^\circ$ spatial and three-hourly temporal resolution. The resulting sensitivity matrix is used to link the surface level explanatory variables with observed variations in atmospheric CO₂ concentrations as well as to estimate CO₂ fluxes as part of the inverse model. The WRF-STILT model has been used extensively for atmospheric inverse modeling studies on regional to continental domains (e.g., Fang et al., 2014; Gerbig et al., 2003; Gourdji et al., 2010, 2012; Miller et al., 2013).

3.1. Explanatory Variable Evaluation

The first analysis evaluates the ability of the explanatory variables to capture the spatiotemporal patterns of NEE, as seen through the variations in the atmospheric CO₂ data. To do this, we use a multiple linear regression framework (hereafter “regression model”) that represents the atmospheric observations as a linear combination of atmospheric tracers that are based on the space-time patterns of the explanatory variables. In effect, the transport model is used to translate the space-time patterns of the explanatory variables, which are defined at the Earth surface, into an atmospheric tracer with emissions defined by the space-time patterns of a given explanatory variable:

$$\mathbf{z} = \mathbf{H}\mathbf{X}\boldsymbol{\beta}_{MLR} + \boldsymbol{\varepsilon} \quad (1)$$

where \mathbf{z} is an $(n \times 1)$ vector of three-hourly atmospheric observations (ppm), \mathbf{H} is an $(n \times m)$ sensitivity matrix discussed above and derived from the transport model ($\text{ppm}/(\mu\text{mol}/\text{m}^2\text{s})$) with n being the number of atmospheric observations and m the number of discretized fluxes in space and time, \mathbf{X} is an $(m \times p)$ matrix containing p different explanatory variables (which vary at $1^\circ \times 1^\circ$ spatial and 15 or 16 day temporal resolution) along with a constant term, $\boldsymbol{\beta}_{MLR}$ is a $(p \times 1)$ vector of unknown coefficients that characterize the relationship between the tracers (e.g., $\mathbf{H}\mathbf{X}_{SIF}$) and observations \mathbf{z} , and $\boldsymbol{\varepsilon}$ represents the residuals (ppm), which incorporate both model-data mismatch errors (i.e., observation, aggregation, representation, and transport model errors) and the portion of the flux space-time variability that cannot be explained using the variables in \mathbf{X} .

This framework evaluates the linear relationship between the surface explanatory variables and NEE, as seen through the atmospheric observations. While a simplification, linear relationships have been shown to capture a substantial proportion of the space-time variability in NEE (Fang & Michalak, 2015; Mueller et al., 2010). This regression model also allows for a straightforward assessment of the explanatory power of each explanatory variable. Hence, we can identify and compare each explanatory variable’s ability to explain the variability in NEE as seen through the atmospheric observations, via the coefficient of determination (r^2). We perform an exhaustive search over all possible combinations of explanatory variables to identify the combinations, or regression models, that best explain the atmospheric observations for a given model size. Lastly, we calculate the 95% confidence intervals of the coefficient of determination values using a bootstrap method (Ohtani, 2000).

3.2. Geostatistical Inverse Modeling

The second analysis is designed to explore the impacts of the SIF information on estimates of NEE for North America. To do so, we set up two inverse models, one that incorporates SIF as an explanatory variable and ones that does not. Atmospheric inverse modeling relies on the concept that atmospheric observations are influenced by fluxes at the Earth’s surface as the air passes over an upwind region. With knowledge of background concentrations of the air entering the domain of interest and the path that air parcels take on their way to observation sites, estimates of the most likely distribution of surface fluxes can be obtained.

The geostatistical inverse modeling (GIM) framework allows for the incorporation of explanatory variables and is used here to estimate NEE fluxes at a $1^\circ \times 1^\circ$ spatial and three-hourly temporal resolution for 2008 to 2010 over North American land, with the domain spanning 10° – 70°N and 50° – 170°W . The explanatory variables used in the inversion take the place of a traditional prior flux estimate (typically output from a terrestrial biospheric model (TBM)) and are selected here based on the regression analysis as those variables that provide the largest explanatory power (R^2). We estimate fluxes at a high resolution to minimize spatial and temporal aggregation errors (Gourdji et al., 2010; Kaminski et al., 2001). While flux estimates for individual grid cells and time steps are not considered well constrained by the atmospheric observations, results are ultimately interpreted at monthly and biome scales or greater, via aggregation of a posteriori estimates.

We obtain flux estimates by minimizing the GIM objective function (Michalak et al., 2004):

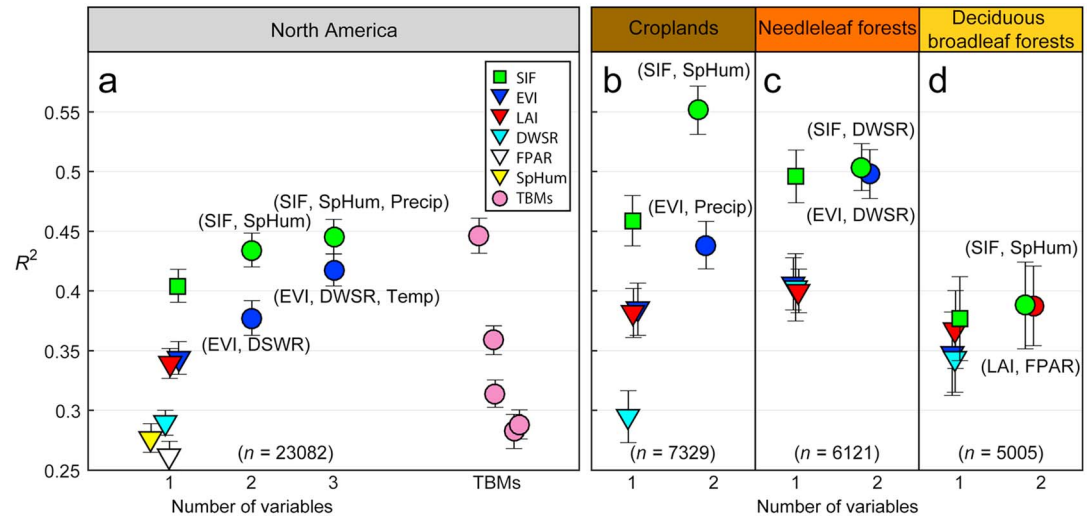


Figure 1. (a) SIF (green square) explains 40% of the variance in the atmospheric CO_2 data from 2008 to 2010 for all of North America; regionally, SIF explains 46%, 50%, and 38% of the variance in atmospheric observations primarily sensitive to the (b) croplands, (c) needleleaf forests, and (d) deciduous broadleaf forests, respectively (see Figure 2b for biome map). Also shown are the best multivariable regression models with SIF (green circles) and without SIF (circles colored based on first-listed variable). The error bars represent 95% confidence intervals obtained from bootstrapping. Variables and models explaining less than 25% of the variance not shown.

$$L_{s,\beta} = \frac{1}{2}(\mathbf{z} - \mathbf{H}\mathbf{s})^T \mathbf{R}^{-1}(\mathbf{z} - \mathbf{H}\mathbf{s}) + \frac{1}{2}(\mathbf{s} - \mathbf{X}\boldsymbol{\beta}_{GIM})^T \mathbf{Q}^{-1}(\mathbf{s} - \mathbf{X}\boldsymbol{\beta}_{GIM}) \quad (2)$$

where \mathbf{s} ($m \times 1$) represents a vector of unknown discretized surface fluxes in space and time ($\mu\text{mol}/\text{m}^2\text{s}$) \mathbf{H} , \mathbf{X} and \mathbf{z} are explained in section 3.1, \mathbf{Q} is the ($m \times m$) prior error covariance matrix ($(\mu\text{mol}/\text{m}^2\text{s})^2$), and \mathbf{R} is the ($n \times n$) model-data mismatch covariance matrix (ppm^2). As implemented here, this framework simultaneously estimates the space and time varying unknown surface fluxes, \mathbf{s} , as well as a unique scalar coefficients, $\boldsymbol{\beta}_{GIM}$, for each explanatory variable over the entire space and time domain informed by the entire network of atmospheric observations, similar to Gourdji et al. (2012). Refer to Gourdji et al. (2012) for further details regarding the specifics of the GIM framework including the estimation of covariance parameters for the \mathbf{Q} and \mathbf{R} matrices. The framework developed for this work is targeted to specifically address and therefore isolate the additional information provided by the explanatory variables in \mathbf{X} ; hence, \mathbf{Q} and \mathbf{R} parameters are held constant between the two inverse models with and without SIF. Both analyses are informed by the same atmospheric CO_2 observations, leverage the same transport model, and cover the same analysis domain (see supporting information Table S3 for details of the differences between the regression and inversion analyses).

4. Results and Discussion

A tracer defined by the spatiotemporal patterns of SIF explains a substantial portion of the variability ($\sim 40\%$) in the atmospheric observations over North America, more so than any other explanatory variable (Figure 1a). While SIF has been shown to track GPP at the plot scale (e.g., Guanter et al., 2014; Joiner et al., 2014), here we show that SIF correlates strongly with space-time patterns of NEE at $1^\circ \times 1^\circ$ spatial resolution across a range of biomes in North America. The fact that just this one variable explains close of half of the observed variability in atmospheric observations in North America across 3 years is both surprising and encouraging and is consistent with the fact that GPP itself explains a substantial portion of variability in NEE (Baldocchi, 2008).

The explanatory power of a tracer defined by SIF is greater than that of all other examined explanatory variables, and even greater than a majority of NEE estimates from 10 terrestrial biospheric models (TBMs) participating in the Multiscale synthesis and Terrestrial Model Intercomparison Project (MSTMIP) project (Huntzinger et al., 2013, 2014) (see details in supporting information Text S1). We note that while the TBMs were not calibrated to this set of atmospheric observations, TBMs incorporate more sophisticated mechanistic knowledge of the processes controlling GPP and ecosystem respiration (R_{eco}). The fact that the examined explanatory variables can rival the explanatory power of mechanistic models supports the notion that

relatively simple regression models can be used to explore the surface level drivers of NEE fluxes at regional scales (Figures 1 and S1).

Because SIF is a corollary for GPP and not R_{eco} , we explore whether the relative performance of SIF might be impacted by the addition of other explanatory variables related to temperature and moisture, known drivers of R_{eco} . By performing an exhaustive search among the explanatory variables listed in section 2.2 to find the best (highest R^2) combination of variables, we find that variables associated with R_{eco} significantly improve the fit of the regression models over their respective single-variable variants (Figure 1a). Even with the additional variables, the benefit of including SIF remains at the two and three-variable regression model level (Figure 1a). Coupling SIF with specific humidity (SpHum), a measure of the moisture content or mass of water vapor per unit mass of air, yields the greatest increase in the variance explained ($R^2 = 0.43$). The identification of specific humidity as an important covariate for NEE over North America aligns with previous inverse modeling work by Gourdji et al. (2012), who found that specific humidity was correlated with a respiratory signal and improved NEE estimates over North America. Specific humidity modifies the continental seasonal cycle via reductions (increases) in the magnitude of growing season (dormant season) NEE, which act as simplified R_{eco} adjustments to the SIF-only regression model (Figure S2). Specific humidity, by incorporating information of both temperature and moisture, can be seen as a broad explanatory factor of heterotrophic respiration (Davidson et al., 2006; Ise & Moorcroft, 2006; Wei et al., 2015), although the underlying mechanisms are admittedly much more complex. Augmenting the two variable SIF regression model further by including precipitation provides only marginal benefit (Figure 1a).

Coupling EVI (the best non-SIF explanatory variable) with downwelling shortwave radiation (DWSR) also improves the fit ($R^2 = 0.38$) but this combination still explains less variability than SIF alone ($r^2 = 0.40$). While DWSR is not a driver of R_{eco} it likely acts to adjust the space-time patterns of EVI to better reflect the NEE signal. The three-variable regression model of EVI, DWSR, and temperature further increases the variance explained ($R^2 = 0.42$) such that these three variables together provide comparable explanatory power to SIF alone. This combination of EVI, DWSR, and temperature, while simple, aligns with site-level studies that showed that a combination of leaf area, temperature, and radiation can explain a similar portion of the variability in NEE as observed here (van Dijk et al., 2005). Using these regression models, we see that the space-time patterns of SIF are able to explain NEE variability across North America. In order to assess variations between biomes, a similar analysis is conducted at the biome scale.

A regional analysis shows a clear biome dependence in SIF's ability to explain NEE (over existing vegetation indices), with the largest improvements seen in the croplands and needleleaf forests (Figures 1b and 1c). We subdivide observations using the transport model to identify the dominant biome of influence for any given observation (Figure S3). When taken alone, SIF explains more variability than other explanatory variables in croplands and needleleaf forests ($\Delta r^2 = 0.07$ and $\Delta r^2 = 0.09$, respectively). This provides the first biome-level atmospheric observation-driven indication that SIF tracks GPP better than existing vegetation indices in croplands and needleleaf forests, which had previously been hypothesized based on analyses using plot-scale and terrestrial model-based GPP estimates (Guanter et al., 2014; Walther et al., 2015; Zhang et al., 2016). In deciduous broadleaf forests, on the other hand, SIF performs similarly to existing vegetation indices, which aligns with recent work (Walther et al., 2015) showing that SIF and EVI both track modeled GPP equally well in deciduous forests.

The superior explanatory power of SIF over existing vegetation indices in croplands and needleleaf forests is driven primarily by a better representation of seasonality (Figures S4 and S5). In croplands, SIF is needed to explain the unique short and intense peak of the growing season (typical of cropland NEE) (Figure S4). The advantage in explanatory power remains in the two-variable cropland regression model (SIF and SpHum) (Figure 1b) showing that the increases in GPP that were derived from site-level SIF-GPP comparisons (e.g., Guanter et al., 2014) are apparent at the biome level and even carry through to the NEE signal. In needleleaf forests, on the other hand, we see that SIF tracks seasonal transitions of NEE better than greenness indicators (Figure S5)—supporting TBM-based findings (Walther et al., 2015) that showed a decoupling of GPP and greenness in these regions. Downwelling shortwave radiation (DWSR) is needed to improve the seasonality and bridge the gap between EVI and SIF, further confirming that seasonality is better captured by SIF (Figures 1c and S5) but also highlighting that more complex regression models without SIF are able to capture this timing.

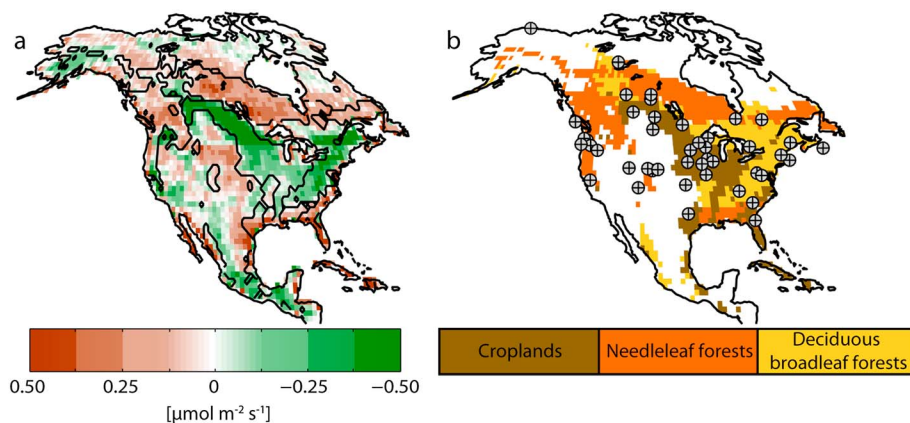


Figure 2. Including SIF information leads to a redistribution of the growing season uptake from needleleaf forests to croplands (a). The difference between June, July, and August flux estimates obtained from inverse models with and without SIF (each using the three explanatory variables from Figure 1a) averaged over 3 years (2008–2010), with green (brown) indicating a stronger (weaker) uptake in the NEE estimates from the inversion including SIF. A biome map with atmospheric observation locations shown as circles with crosses is shown in Figure 2b. Biome outlines are shown as black lines (a). For unit conversion: $100 \text{ gC/m}^2 \text{ yr} = 0.264 \text{ } \mu\text{mol/m}^2 \text{ s}$.

We acknowledge that the simple regression models we are utilizing do not capture the complexity of the true underlying mechanisms driving NEE; it is nevertheless useful to identify the primary drivers of NEE using an atmospheric observation constraint. Starting with the individual best explanatory variables, SIF and EVI, we see that these both help to capture the major seasonal and spatial patterns of the NEE signal. The regression coefficients associated with these variables indicate that an increase in SIF and EVI is associated with increased uptake of CO_2 , as expected (equation (1)). When moving from the single-variable regression models to the multivariable regression models, we see that the added variables are known drivers of R_{eco} . We also find that sign of the regression coefficients on these variables is opposite to those for SIF or EVI, signifying that these variables are associated with an increase in atmospheric CO_2 or a respiratory signal. Thus, we find that atmospheric observations do provide a constraint on the relationship between explanatory variables and CO_2 exchange. The fact that these variables are understood to be associated with GPP and R_{eco} provides confirmation that the signal in atmospheric observations can be used to identify variables that align with our mechanistic understanding of broad drivers of both photosynthesis and respiration, while adding confidence to our findings regarding the importance of SIF as an explanatory variable of NEE.

Moving from the regression analysis to the inverse models, we see that the unique information SIF provides translates to inferences into the spatial distribution of NEE fluxes over croplands and needleleaf forest regions of North America (Figure 2). The difference map between inverse model estimates including and excluding SIF reveals a consistent difference in the spatial pattern over 3 years (2008 to 2010) (Figure 2). The results in Figure 2 are based on inverse models with three explanatory variables (from Figure 1a) in \mathbf{X} (see equation (2)), but similar results are found using two explanatory variables (from Figure 1a) (Figures S6 and S7). It is important to note that no prior information on biome classification was provided in the inverse models, making the correspondence of the differences in NEE estimates with the croplands and needleleaf forest biome regions striking (biomes defined by an IGBP landcover classification map (Figure 2b) (Frankenberg et al., 2011)). Spatially, SIF is informing a shift in the subcontinental distribution of CO_2 fluxes within North America.

Aggregating fluxes by biome reveals that a redistribution of NEE from the needleleaf forests to croplands is statistically significant at the annual level and more pronounced over the growing season (Figures 3a and 3b) (differences in other biomes are not statistically significant ($p > 0.01$)). Even at the monthly scale we see that the addition of SIF significantly alters the cropland and needleleaf forest biome level flux estimates during the peak summer months. We further probe the robustness of the inverse modeling results (see the Sensitivity Analysis section in the supporting information Text S1) and find that the overall conclusion about the difference between inversions with and without SIF is insensitive to both background conditions and choice of fossil fuel inventory. Thus, by focusing on the difference between inversions, we find that

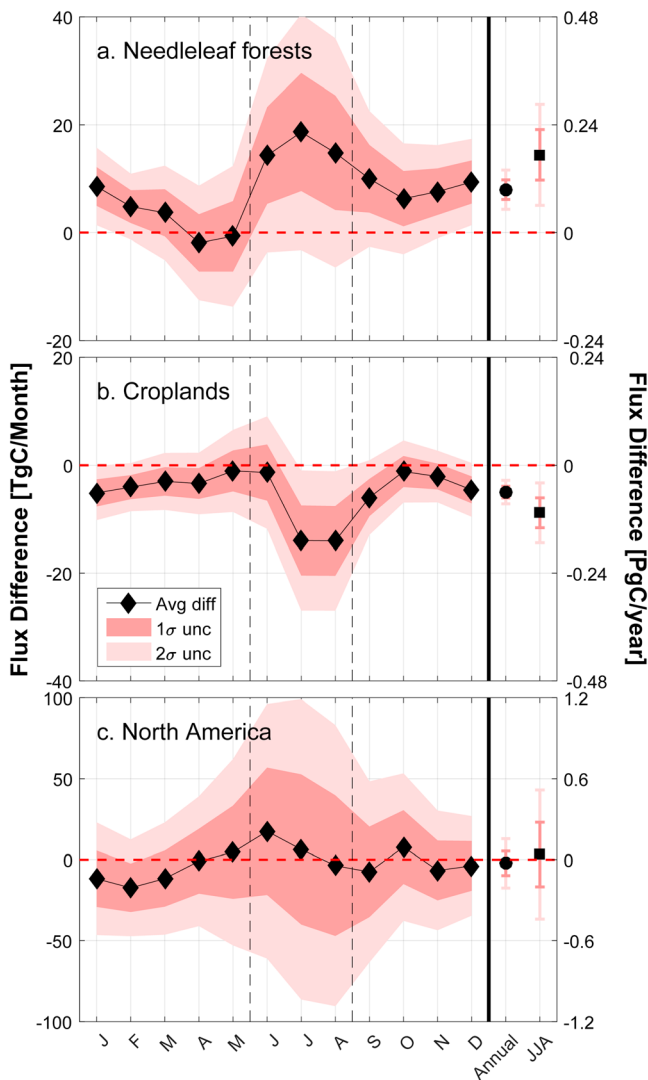


Figure 3. The redistribution of uptake from needleleaf forests to croplands averaged over 3 years (2008–2010) is statistically significant at the annual level and June, July, and August (JJA). Monthly (black diamonds), annual (black circles), and JJA (black squares) differences in flux estimates between the inverse models with and without SIF, aggregated over (a and b) two biomes and (c) all of North America with one standard deviation (dark shading) and two standard deviation (light shading) uncertainty bounds (uncertainty propagation for the difference between two averages is calculated using the posterior uncertainty estimates from the with-SIF and without-SIF inversions for all 3 years). Negative (positive) values represent more (less) uptake in the estimates from the inversion including SIF. Biomes not shown had differences that were not statistically significant at the biome-monthly or biome-annual level ($p > 0.01$).

local influences), (4) boundary conditions, and (5) transport model errors. Some issues are a part of any exploration into the biosphere using atmospheric observations (e.g., 3 and 5) and are the reason for objectively estimating and incorporating the error terms in equations (1) and (2). Some issues specifically affect regional inverse modeling studies (e.g., 4) and were explored in the supporting information Text S1 (see Sensitivity Analysis section). For 1 and 2, we use atmospheric observations averaged over 3 h in the midafternoon as transport models typically best represent these times of the day, yet attempting to fit fluctuations in three-hourly atmospheric observations with 16 day explanatory variables is admittedly difficult. We justify keeping the high-frequency atmospheric observations because it allows us to examine changes in the surface influence of the data, which is crucial for minimizing aggregation errors in the inverse model, which

including SIF in an inverse model constrained by atmospheric observations leads to a robust difference in NEE in both the needleleaf forests and croplands.

The spatial shift in the NEE estimates resulting from the use of SIF provides the first large-scale perspective of the impacts of SIF in defining subcontinental patterns of carbon exchange that is informed by a large-scale atmospheric observation constraint. The additional uptake in the croplands along with the compensating reduction in the sink in the needleleaf forests offers confirmation of findings (in this case at the continental scale) of recent flux-tower based studies where state-of-the-art process-based terrestrial biosphere models were found to underestimate GPP in croplands (Guanter et al., 2014) and overestimate GPP in needleleaf forests (A. D. Richardson et al., 2012). As NEE in croplands is largely driven by the seasonal pattern of GPP, the increase in net uptake we see when including SIF offers a large-scale validation of the increase in GPP seen in previous work (Guan et al., 2016; Guanter et al., 2014). The fact that SIF informs a decrease in the net uptake in needleleaf forests supports the notion that SIF, by being more directly linked to the photosynthetic machinery (i.e., incorporating the influences of FPAR, PAR, and light-use efficiency), is superior to vegetative data sets when attempting to predict the space-time patterns of CO₂ flux in these forested regions (Jeong et al., 2017; Luus et al., 2017; Walther et al., 2015; Yang et al., 2015, 2016). We speculate that the SIF-informed shift in NEE away from the boreal region seen here may also explain why there has historically been a tendency for inverse models to overestimate northern hemisphere extratropical terrestrial carbon uptake (Sarmiento et al., 2010; Stephens et al., 2007), although an expanded global analysis similar to that of Parazoo et al. (2014) but for NEE would be needed to confirm this. As most inverse models rely on TBM output as an initial guess or “prior,” the inability of TBMs to adequately capture the seasonality of boreal regions hampers the ability of inverse models to accurately partition NEE geographically. Interestingly, at the continental scale, the inverse models with and without SIF yield nearly identical estimates at both monthly and annual scales (Figure 3), indicating that while the total large-scale carbon budget is determined primarily by the constraint provided by the atmospheric observations, SIF provides crucial information for allocating NEE at intermediate scales.

Lastly, we acknowledge that a variety of other complexities exist that likely impact the ability to explain the NEE signal using atmospheric observations. These include (1) merging of surface signals from differing space/time regions, (2) higher temporal resolution of atmospheric observations (three-hourly) compared to surface level explanatory variables (16 day), (3) atmospheric data issues (e.g., lack of coverage and

Acknowledgments

This work is funded by the National Aeronautics and Space Administration (NASA) under grants NNH14AY371, NNH16AC911, NNX12AB90G, NNX12AM97G, and NNX13AC48G. The MODIS MOD13C1-EVI data product is courtesy of the online Data Pool at the NASA Land Processes Distributed Active Archive Center (LP DAAC), USGS/Earth Resources Observation and Science (EROS) Center, Sioux Falls, South Dakota (https://lpdaac.usgs.gov/data_access). We thank C.J. Tucker and J. Pinzon of NASA GSFC for making available the GIMMS NDVI 3g data set and the Boston University Vegetation Remote Sensing and Climate Research group for providing the LAI 3g, and FPAR 3g data sets. Atmospheric and Environmental Research Inc. (AER), and in particular Thomas Nehrkorn, John Henderson, and Janusz Eluzkiewicz, performed the WRF-STILT simulations and provided the sensitivity footprints. Funding for the Multi-scale synthesis and Terrestrial Model Intercomparison Project (MsTMIP; <http://nacp.ornl.gov/MsTMIP.shtml>) activity was provided through NASA ROSES grant NNX10AG01A. Data management support for preparing, documenting, and distributing model driver and output data was performed by the Modeling and Synthesis Thematic Data Center at Oak Ridge National Laboratory (ORNL; <http://nacp.ornl.gov>), with funding through NASA ROSES grant NNH10AN681. Finalized MsTMIP data products are archived at the ORNL DAAC (<http://daac.ornl.gov>). We gratefully acknowledge the efforts of the PIs of the various towers providing continuous atmospheric CO₂ observations, which were instrumental for these analyses. The sites BRW, WGC, SNP, SCT, AMT, WBI, BAO, LEF, and WKT are part of NOAA's Global Greenhouse Gas Reference Network operated by the Global Monitoring Division of NOAA's Earth System Research Laboratory with additional support from NOAA's Climate Program Office and are a contribution to the North American Carbon Program. The installation of CO₂ sampling equipment was made possible at AMT, by a grant from the National Science Foundation Biocomplexity in the Environment Program (ATM-0221850), at SNP, by the University of Virginia, and at SCT by funding provided by the DOE Office of Science-Terrestrial Carbon Processes Program and performed under contract DE-AC09-08SR22470. Savannah River National Laboratory (SNRL) is operated by Savannah River Nuclear Solutions, LLC under contract DE-AC09-08SR22470 with the U.S. Department of Energy. WGC measurements were supported by a combination of the California Energy

estimates fluxes at a three-hourly resolution (see Gourdji et al., 2010; Kaminski et al., 2001). Nevertheless, by coupling the network of atmospheric observations with SIF, we are given that an unprecedented look into the information SIF is providing at intermediate scales for explaining the space-time patterns of NEE across North America.

5. Conclusions

In this study, we show that SIF can explain a substantial portion of the space-time variability of NEE at regional ($1^\circ \times 1^\circ$) scales throughout North America and within specific biomes, more than other existing vegetation and climate indicators. We use a network of atmospheric CO₂ observations to link regional-scale NEE to SIF and find that the ability of SIF to represent GPP provides valuable information for explaining NEE across North America. Through a regression analysis, we find that patterns of SIF are indeed consistent with the NEE signal observed in the atmosphere, more so than a variety of existing vegetation indices and even TBMs. These results offer the first example of using a network of CO₂ observations to evaluate the utility of SIF in representing the spatiotemporal variability of NEE for regional to continental domains. The inversion analyses further show that SIF provides new insight into the spatial allocation of continental-scale growing season NEE between subcontinental regions associated with the cropland and needleleaf forest biomes in North America and that these shifts are indeed more consistent with the observed atmospheric CO₂ record. More broadly, we show that atmospheric CO₂ data provide a useful tool for exploring flux drivers at difficult to measure yet crucial intermediate scales.

References

- Asefi-Najafabady, S., Rayner, P. J., Gurney, K. R., McRobert, A., Song, Y., Coltin, K., ... Baugh, K. (2014). A multiyear, global gridded fossil fuel CO₂ emission data product: Evaluation and analysis of results. *Journal of Geophysical Research: Atmospheres*, *119*, 10,213–10,231. <https://doi.org/10.1002/2013JD021296>
- Baldocchi, D. (2008). TURNER REVIEW No. 15. 'Breathing' of the terrestrial biosphere: Lessons learned from a global network of carbon dioxide flux measurement systems. *Australian Journal of Botany*, *56*(1), 1–26. <https://doi.org/10.1071/BT07151>
- Barman, R., Jain, A. K., & Liang, M. (2014a). Climate-driven uncertainties in modeling terrestrial energy and water fluxes: A site-level to global-scale analysis. *Global Change Biology*, *20*(6), 1885–1900. <https://doi.org/10.1111/gcb.12473>
- Barman, R., Jain, A. K., & Liang, M. (2014b). Climate-driven uncertainties in modeling terrestrial gross primary production: A site level to global-scale analysis. *Global Change Biology*, *20*(5), 1394–1411. <https://doi.org/10.1111/gcb.12474>
- Davidson, E. A., Janssens, I. A., & Luo, Y. (2006). On the variability of respiration in terrestrial ecosystems: Moving beyond Q10. *Global Change Biology*, *12*(2), 154–164. <https://doi.org/10.1111/j.1365-2486.2005.01065.x>
- Fang, Y., & Michalak, A. M. (2015). Atmospheric observations inform CO₂ flux responses to environmental drivers. *Global Biogeochemical Cycles*, *29*, 555–566. <https://doi.org/10.1002/2014GB005034>
- Fang, Y., Michalak, A. M., Shiga, Y. P., & Yadav, V. (2014). Using atmospheric observations to evaluate the spatiotemporal variability of CO₂ fluxes simulated by terrestrial biospheric models. *Biogeosciences*, *11*(23), 6985–6997. <https://doi.org/10.5194/bg-11-6985-2014>
- Frankenberg, C., Fisher, J. B., Worden, J., Badgley, G., Saatchi, S. S., Lee, J. E., ... Yokota, T. (2011). New global observations of the terrestrial carbon cycle from GOSAT: Patterns of plant fluorescence with gross primary productivity. *Geophysical Research Letters*, *38*, L17706. <https://doi.org/10.1029/2011GL048738>
- Friedlingstein, P., Meinshausen, M., Arora, V. K., Jones, C. D., Anav, A., Liddicoat, S. K., & Knutti, R. (2014). Uncertainties in CMIP5 Climate Projections due to Carbon Cycle Feedbacks. *Journal of Climate*, *27*(2), 511–526. <https://doi.org/10.1175/JCLI-D-12-00579.1>
- Gerbig, C., Lin, J. C., Wofsy, S. C., Daube, B. C., Andrews, A. E., Stephens, B. B., ... Grainger, C. A. (2003). Toward constraining regional-scale fluxes of CO₂ with atmospheric observations over a continent: 1. Observed spatial variability from airborne platforms. *Journal of Geophysical Research*, *108*(D24), 4756. <https://doi.org/10.1029/2002JD003018>
- Gloor, M., Bakwin, P., Hurst, D., Lock, L., Draxler, R., & Tans, P. (2001). What is the concentration footprint of a tall tower? *Journal of Geophysical Research*, *106*(D16), 17,831–17,840. <https://doi.org/10.1029/2001JD900021>
- Göckede, M., Michalak, A. M., Vickers, D., Turner, D. P., & Law, B. E. (2010). Atmospheric inverse modeling to constrain regional-scale CO₂ budgets at high spatial and temporal resolution. *Journal of Geophysical Research*, *115*, D15113. <https://doi.org/10.1029/2009JD012257>
- Gourdji, S. M., Hirsch, A. I., Mueller, K. L., Yadav, V., Andrews, A. E., & Michalak, A. M. (2010). Regional-scale geostatistical inverse modeling of north American CO(2) fluxes: A synthetic data study. *Atmospheric Chemistry and Physics*, *10*(13), 6151–6167. <https://doi.org/10.5194/acp-10-6151-2010>
- Gourdji, S. M., Mueller, K. L., Yadav, V., Huntzinger, D. N., Andrews, A. E., Trudeau, M., ... Michalak, A. M. (2012). North American CO₂ exchange: Inter-comparison of modeled estimates with results from a fine-scale atmospheric inversion. *Biogeosciences*, *9*(1), 457–475. <https://doi.org/10.5194/bg-9-457-2012>
- Griffis, T. J., Sargent, S. D., Baker, J. M., Lee, X., Tanner, B. D., Greene, J., ... Billmark, K. (2008). Direct measurement of biosphere-atmosphere isotopic CO₂ exchange using the eddy covariance technique. *Journal of Geophysical Research*, *113*, D08304. <https://doi.org/10.1029/2007JD009297>
- Guan, K., Berry, J. A., Zhang, Y., Joiner, J., Guanter, L., Badgley, G., & Lobell, D. B. (2016). Improving the monitoring of crop productivity using spaceborne solar-induced fluorescence. *Global Change Biology*, *22*(2), 716–726. <https://doi.org/10.1111/gcb.13136>
- Guanter, L., Zhang, Y., Jung, M., Joiner, J., Voigt, M., Berry, J. A., ... Griffis, T. J. (2014). Global and time-resolved monitoring of crop photosynthesis with chlorophyll fluorescence. *Proceedings of the National Academy of Sciences of the United States of America*, *111*(14), E1327–E1333. <https://doi.org/10.1073/pnas.1320008111>

Commission's Public Interest

Environmental Research Program to the Lawrence Berkeley National Laboratory under contract DE-AC02-05CH11231 and NOAA. Research at ACV, AOZ, RKW, RCE, RMM, RRL, and RGV was sponsored by the U.S. Department of Energy Office of Science TCP program (DE-FG02-06ER64315) and by the U.S. Department of Commerce, NOAA Office of Global Programs (NA08OAR4310533). The five Oregon sites OFR, OMT, OYQ, OMP, and ONG were supported by NOAA (NA11OAR4310056). We thank the following individuals for collecting and providing the atmospheric CO₂ data from the following sites: Arlyn Andrews (NOAA) for AMT, WBI, BAO, LEF, and WKT; Arlyn Andrews (NOAA) and Stephan De Wekker (UVA) for SNP; Kirk Thoning (NOAA) and Pieter Tans (NOAA) for BRW; Arlyn Andrews (NOAA) and Matt J. Parker (SRNL) for SCT; Marc Fischer (LBNL) and Arlyn Andrews (NOAA) for WGC; Kenneth Davis, Scott Richardson, and Natasha Miles (The Pennsylvania State University) for ACV, AOZ, RKW, RCE, RMM, RRL, and RGV; Britton Stephens (NCAR) and the Regional Atmospheric Continuous CO₂ Network in the Rocky Mountains (RACCOON) for NWR, SPL, RBA, and HDP; Beverly Law (Oregon State University), Andres Schmidt (RWTH Aachen University), and the TERRA-PNW group for data from five Oregon sites, OFR, OMT, OYQ, OMP, and ONG; William Munger (Harvard University) and Steven Wofsy (Harvard University) for HFM; Doug Worthy (Environment Canada) for CDL, FRD, WSA, EGB, ETL, LLB, CHI, BCK, ESP, EST, and BRA; Tim Griffis (UMN) for KCMP; Colm Sweeney (NOAA) for MVY; and Sebastien Biraud (LBNL) and Margaret Torn (LBNL) for SGP. Readers can contact individual data providers for site-specific CO₂ concentrations or the author (yshiga@stanford.edu) to access the other data and methods used in this study.

- Gurney, K. R., Law, R. M., Denning, A. S., Rayner, P. J., Baker, D., Bousquet, P., ... Yuen, C. W. (2002). Towards robust regional estimates of CO₂ sources and sinks using atmospheric transport models. *Nature*, *415*(6872), 626–630. <https://doi.org/10.1038/415626a>
- Huete, A., Didan, K., Miura, T., Rodriguez, E., Gao, X., & Ferreira, L. (2002). Overview of the radiometric and biophysical performance of the MODIS vegetation indices. *Remote Sensing of Environment*, *83*(1-2), 195–213. [https://doi.org/10.1016/S0034-4257\(02\)00096-2](https://doi.org/10.1016/S0034-4257(02)00096-2)
- Huntzinger, D. N., Schwalm, C., Michalak, A. M., Schaefer, K., King, A. W., Wei, Y., ... Zhu, Q. (2013). The North American Carbon Program Multi-Scale Synthesis and Terrestrial Model Intercomparison Project—Part 1: Overview and experimental design. *Geoscientific Model Development*, *6*(6), 2121–2133. <https://doi.org/10.5194/gmd-6-2121-2013>
- Huntzinger, D. N., Schwalm, C. R., Wei, Y., Cook, R. B., Michalak, A. M., Schaefer, K., ... Zhu, Q. (2014). NACP MsTMIP: Global 0.5-deg terrestrial biosphere model outputs in standard format. <https://doi.org/10.3334/ORNLAAC/1225>
- Ise, T., & Moorcroft, P. R. (2006). The global-scale temperature and moisture dependencies of soil organic carbon decomposition: An analysis using a mechanistic decomposition model. *Biogeochemistry*, *80*(3), 217–231. <https://doi.org/10.1007/s10533-006-9019-5>
- Ito, A. (2010). Changing ecophysiological processes and carbon budget in East Asian ecosystems under near-future changes in climate: Implications for long-term monitoring from a process-based model. *Journal of Plant Research*, *123*(4), 577–588. <https://doi.org/10.1007/s10265-009-0305-x>
- Jain, A. K., Ksheshgi, H. S., & Wuebbles, D. J. (1996). A globally aggregated reconstruction of cycles of carbon and its isotopes. *Tellus B*, *48*(4), 583–600. <https://doi.org/10.1034/j.1600-0889.1996.t01-1-00012.x>
- Jeong, S.-J., Schimel, D., Frankenberg, C., Drewry, D. T., Fisher, J. B., Verma, M., ... Joiner, J. (2017). Application of satellite solar-induced chlorophyll fluorescence to understanding large-scale variations in vegetation phenology and function over northern high latitude forests. *Remote Sensing of Environment*, *190*, 178–187. <https://doi.org/10.1016/j.rse.2016.11.021>
- Joiner, J., Yoshida, Y., Vasilkov, A. P., Yoshida, Y., Corp, L. A., & Middleton, E. M. (2011). First observations of global and seasonal terrestrial chlorophyll fluorescence from space. *Biogeosciences*, *8*(3), 637–651. <https://doi.org/10.5194/bg-8-637-2011>
- Joiner, J., Guanter, L., Lindstrot, R., Voigt, M., Vasilkov, A. P., Middleton, E. M., ... Frankenberg, C. (2013). Global monitoring of terrestrial chlorophyll fluorescence from moderate spectral resolution near-infrared satellite measurements: Methodology, simulations, and application to GOME-2. *Atmospheric Measurement Techniques Discussions*, *6*(2), 3883–3930. <https://doi.org/10.5194/amtd-6-3883-2013>
- Joiner, J., Yoshida, Y., Vasilkov, A. P., Schaefer, K., Jung, M., Guanter, L., ... Belelli Marchesini, L. (2014). The seasonal cycle of satellite chlorophyll fluorescence observations and its relationship to vegetation phenology and ecosystem atmosphere carbon exchange. *Remote Sensing of Environment*, *152*, 375–391. <https://doi.org/10.1016/j.rse.2014.06.022>
- Kaminski, T., Rayner, P. J., Heimann, M., & Enting, I. G. (2001). On aggregation errors in atmospheric transport inversions. *Journal of Geophysical Research*, *106*(D5), 4703–4715. <https://doi.org/10.1029/2000JD900581>
- Keeling, C. D., Bacastow, R. B., Bainbridge, A. E., Ekdahl, C. A., Guenther, P. R., Waterman, L. S., & Chin, J. F. S. (1976). Atmospheric carbon dioxide variations at Mauna Loa Observatory, Hawaii. *Tellus*, *28*(6), 538–551. <https://doi.org/10.1111/j.2153-3490.1976.tb00701.x>
- King, A. W., Post, W. M., & Wullschlegel, S. D. (1997). The potential response of terrestrial carbon storage to changes in climate and atmospheric CO₂. *Climatic Change*, *35*(2), 199–227. <https://doi.org/10.1023/A:1005317530770>
- Krinner, G., Viovy, N., de Noblet-Ducoudré, N., Ogee, J., Polcher, J., Friedlingstein, P., ... Prentice, I. C. (2005). A dynamic global vegetation model for studies of the coupled atmosphere-biosphere system. *Global Biogeochemical Cycles*, *19*, GB1015. <https://doi.org/10.1029/2003GB002199>
- Lauvaux, T., Schuh, A. E., Uliasz, M., Richardson, S., Miles, N., Andrews, A. E., ... Davis, K. J. (2012). Constraining the CO₂ budget of the corn belt: Exploring uncertainties from the assumptions in a mesoscale inverse system. *Atmospheric Chemistry and Physics*, *12*(1), 337–354. <https://doi.org/10.5194/acp-12-337-2012>
- Le Quéré, C., Andrew, R. M., Canadell, J. G., Sitch, S., Korsbakken, J. I., Peters, G. P., ... Zaehle, S. (2016). Global Carbon Budget 2016. *Earth System Science Data*, *8*(8), 605–649. <https://doi.org/10.5194/essd-8-605-2016>
- Li, H., Huang, M., Wigmosta, M. S., Ke, Y., Coleman, A. M., Leung, L. R., ... Ricciuto, D. M. (2011). Evaluating runoff simulations from the Community Land Model 4.0 using observations from flux towers and a mountainous watershed. *Journal of Geophysical Research*, *116*, D24120. <https://doi.org/10.1029/2011JD016276>
- Lin, J. C., Gerbig, C., Wofsy, S. C., Andrews, A. E., Daube, B. C., Davis, K. J., & Grainger, C. A. (2003). A near-field tool for simulating the upstream influence of atmospheric observations: The Stochastic Time-Inverted Lagrangian Transport (STILT) model. *Journal of Geophysical Research*, *108*(D16), 4493. <https://doi.org/10.1029/2002JD003161>
- Lin, J. C., Mallia, D. V., Wu, D., & Stephens, B. B. (2017). How can mountaintop CO₂ observations be used to constrain regional carbon fluxes? *Atmospheric Chemistry and Physics*, *17*(9), 5561–5581. <https://doi.org/10.5194/acp-17-5561-2017>
- Lus, K. A., Commane, R., Parazoo, N. C., Benmergui, J., Euskirchen, E. S., Frankenberg, C., ... Lin, J. C. (2017). Tundra photosynthesis captured by satellite-observed solar-induced chlorophyll fluorescence. *Geophysical Research Letters*, *44*, 1564–1573. <https://doi.org/10.1002/2016GL070842>
- Magnani, F., Raddi, S., Mohammed, G., & Middleton, E. M. (2014). Let's exploit available knowledge on vegetation fluorescence. *Proceedings of the National Academy of Sciences of the United States of America*, *111*(25), E2510–E2510. <https://doi.org/10.1073/pnas.1406600111>
- Mao, J., Thornton, P. E., Shi, X., Zhao, M., & Post, W. M. (2012). Remote sensing evaluation of CLM4 GPP for the period 2000–09. *Journal of Climate*, *25*(15), 5327–5342. <https://doi.org/10.1175/JCLI-D-11-00401.1>
- Mesinger, F., DiMego, G., Kalnay, E., Mitchell, K., Shafran, P. C., Ebisuzaki, W., ... Shi, W. (2006). North American Regional Reanalysis. *Bulletin of the American Meteorological Society*, *87*(3), 343–360. <https://doi.org/10.1175/BAMS-87-3-343>
- Michalak, A. M., Bruhwiler, L., & Tans, P. P. (2004). A geostatistical approach to surface flux estimation of atmospheric trace gases. *Journal of Geophysical Research*, *109*, D14109. <https://doi.org/10.1029/2003JD004422>
- Miles, N. L., Richardson, S. J., Davis, K. J., Lauvaux, T., Andrews, A. E., West, T. O., ... Crosson, E. R. (2012). Large amplitude spatial and temporal gradients in atmospheric boundary layer CO₂ mole fractions detected with a tower-based network in the U.S. upper Midwest. *Journal of Geophysical Research*, *117*, G01019. <https://doi.org/10.1029/2011JG001781>
- Miles, N. L., Richardson, S. J., Davis, K. J., Andrews, A. E., Griffis, T. J., Bandaru, V., & Hosman, K. P. (2013). NACP MCI: Tower atmospheric CO₂ concentrations, upper Midwest region, USA, 2007–2009. <https://doi.org/10.3334/ORNLAAC/1202>
- Miller, S. M., Wofsy, S. C., Michalak, A. M., Kort, E. A., Andrews, A. E., Biraud, S. C., ... Sweeney, C. (2013). Anthropogenic emissions of methane in the United States. *Proceedings of the National Academy of Sciences of the United States of America*, *110*(50), 20,018–20,022. <https://doi.org/10.1073/pnas.1314392110>
- Mueller, K. L., Yadav, V., Curtis, P. S., Vogel, C., & Michalak, A. M. (2010). Attributing the variability of eddy-covariance CO₂ flux measurements across temporal scales using geostatistical regression for a mixed northern hardwood forest. *Global Biogeochemical Cycles*, *24*, GB3023. <https://doi.org/10.1029/2009GB003642>

- Myneni, R. B., Hoffman, S., Knyazikhin, Y., Privette, J. L., Glassy, J., Tian, Y., ... Running, S. W. (2002). Global products of vegetation leaf area and fraction absorbed PAR from year one of MODIS data. *Remote Sensing of Environment*, 83(1-2), 214–231. [https://doi.org/10.1016/S0034-4257\(02\)00074-3](https://doi.org/10.1016/S0034-4257(02)00074-3)
- NASA-LP DAAC (2010). NASA Land Processes Distributed Active Archive Center (LP DAAC). MOD13C1. USGS/Earth Resources Observation and Science (EROS) Center, Sioux Falls, South Dakota, 2010.
- Nehrkorn, T., Eluszkiewicz, J., Wofsy, S. C., Lin, J. C., Gerbig, C., Longo, M., & Freitas, S. (2010). Coupled weather research and forecasting–stochastic time-inverted lagrangian transport (WRF–STILT) model. *Meteorology and Atmospheric Physics*, 107(1-2), 51–64. <https://doi.org/10.1007/s00703-010-0068-x>
- ObsPack GLOBALVIEWplus v2.1 (2016). Cooperative Global Atmospheric Data Integration Project, Multi-laboratory compilation of atmospheric carbon dioxide data for the period 1957–2015, obspack_co2_1_GLOBALVIEWplus_v2.1_2016-09-02, NOAA, Earth System Research Laboratory, Global Monitoring Division. <https://doi.org/10.15138/G3059Z>, Retrieved from <https://www.esrl.noaa.gov/gmd/ccgg/obspace/data.php>
- Oda, T., & Maksyutov, S. (2011). A very high-resolution (1 km × 1 km) global fossil fuel CO₂ emission inventory derived using a point source database and satellite observations of nighttime lights. *Atmospheric Chemistry and Physics*, 11(2), 543–556. <https://doi.org/10.5194/acp-11-543-2011>
- Ohtani, K. (2000). Bootstrapping R² and adjusted R² in regression analysis. *Economic Modelling*, 17(4), 473–483. [https://doi.org/10.1016/S0264-9993\(99\)00034-6](https://doi.org/10.1016/S0264-9993(99)00034-6)
- Oleson, W., Slater, A., Stockli, R., Wang, A., Sakaguchi, K., Running, S., ... Lamarque, J.-F. (2010). Technical description of version 4.0 of the Community Land Model (CLM), doi:10.5065/D6FB50WZ. Retrieved from <https://opensky.ucar.edu/islandora/object/technotes%3A493>, Accessed 16 June 2017.
- Parazoo, N. C., Bowman, K., Frankenberg, C., Lee, J. E., Fisher, J. B., Worden, J., ... Gerbig, C. (2013). Interpreting seasonal changes in the carbon balance of southern Amazonia using measurements of XCO₂ and chlorophyll fluorescence from GOSAT. *Geophysical Research Letters*, 40, 2829–2833. <https://doi.org/10.1002/grl.50452>
- Parazoo, N. C., Bowman, K., Fisher, J. B., Frankenberg, C., Jones, D. B. A., Cescatti, A., ... Montagnani, L. (2014). Terrestrial gross primary production inferred from satellite fluorescence and vegetation models. *Global Change Biology*, 20(10), 3103–3121. <https://doi.org/10.1111/gcb.12652>
- Porcar-Castell, A., Tyystjärvi, E., Atherton, J., van der Tol, C., Flexas, J., Pfündel, E. E., ... Berry, J. A. (2014). Linking chlorophyll a fluorescence to photosynthesis for remote sensing applications: Mechanisms and challenges. *Journal of Experimental Botany*, 65(15), 4065–4095. <https://doi.org/10.1093/jxb/eru191>
- Ricciuto, D. M., King, A. W., Dragoni, D., & Post, W. M. (2011). Parameter and prediction uncertainty in an optimized terrestrial carbon cycle model: Effects of constraining variables and data record length. *Journal of Geophysical Research*, 116, G01033. <https://doi.org/10.1029/2010JG001400>
- Richardson, A. D., Anderson, R. S., Arain, M. A., Barr, A. G., Bohrer, G., Chen, G., ... Xue, Y. (2012). Terrestrial biosphere models need better representation of vegetation phenology: Results from the North American Carbon Program Site Synthesis. *Global Change Biology*, 18(2), 566–584. <https://doi.org/10.1111/j.1365-2486.2011.02562.x>
- Richardson, S. J., Miles, N. L., Davis, K. J., Crosson, E. R., Rella, C. W., & Andrews, A. E. (2012). Field testing of cavity ring-down spectroscopy analyzers measuring carbon dioxide and water vapor. *Journal of Atmospheric and Oceanic Technology*, 29(3), 397–406. <https://doi.org/10.1175/JTECH-D-11-00063.1>
- Sarmiento, J. L., Gloor, M., Gruber, N., Beaulieu, C., Jacobson, A. R., Mikaloff Fletcher, S. E., ... Rodgers, K. (2010). Trends and regional distributions of land and ocean carbon sinks. *Biogeosciences*, 7(8), 2351–2367. <https://doi.org/10.5194/bg-7-2351-2010>
- Schuh, A. E., Lauvaux, T., West, T. O., Denning, A. S., Davis, K. J., Miles, N., ... Ogle, S. (2013). Evaluating atmospheric CO₂ inversions at multiple scales over a highly inventoried agricultural landscape. *Global Change Biology*, 19, 1424–1439. <https://doi.org/10.1111/gcb.12141>
- Shiga, Y. P., Michalak, A. M., Gourdj, S. M., Mueller, K. L., & Yadav, V. (2014). Detecting fossil fuel emissions patterns from sub-continental regions using North American in-situ CO₂ measurements. *Geophysical Research Letters*, 41, 4381–4388. <https://doi.org/10.1002/2014GL059684>
- Sitch, S., Smith, B., Prentice, I. C., Arneth, A., Bondeau, A., Cramer, W., ... Venevsky, S. (2003). Evaluation of ecosystem dynamics, plant geography and terrestrial carbon cycling in the LPJ dynamic global vegetation model. *Global Change Biology*, 9(2), 161–185. <https://doi.org/10.1046/j.1365-2486.2003.00569.x>
- Sitch, S., Huntingford, C., Gedney, N., Levy, P. E., Lomas, M., Piao, S. L., ... Woodward, F. I. (2008). Evaluation of the terrestrial carbon cycle, future plant geography and climate-carbon cycle feedbacks using five dynamic global vegetation models (DGVMs). *Global Change Biology*, 14(9), 2015–2039. <https://doi.org/10.1111/j.1365-2486.2008.01626.x>
- Skamarock, W. C., & Klemp, J. B. (2008). A time-split nonhydrostatic atmospheric model for weather research and forecasting applications. *Journal of Computational Physics*, 227(7), 3465–3485. <https://doi.org/10.1016/j.jcp.2007.01.037>
- Stephens, B. B., Gurney, K. R., Tans, P. P., Sweeney, C., Peters, W., Bruhwiler, L., ... Denning, A. S. (2007). Weak northern and strong tropical land carbon uptake from vertical profiles of atmospheric CO₂. *Science*, 316(5832), 1732–1735. <https://doi.org/10.1126/science.1137004>
- Stephens, B. B., Miles, N. L., Richardson, S. J., Watt, A. S., & Davis, K. J. (2011). Atmospheric CO₂ monitoring with single-cell NDIR-based analyzers. *Atmospheric Measurement Techniques*, 4(12), 2737–2748. <https://doi.org/10.5194/amt-4-2737-2011>
- Tadić, J. M., Qiu, X., Yadav, V., & Michalak, A. M. (2015). Mapping of satellite Earth observations using moving window block kriging. *Geoscientific Model Development*, 8(10), 3311–3319. <https://doi.org/10.5194/gmd-8-3311-2015>
- Tadić, J. M., Qiu, X., Miller, S., & Michalak, A. M. (2017). Spatio-temporal approach to moving window block kriging of satellite data v1.0. *Geoscientific Model Development*, 10(2), 709–720. <https://doi.org/10.5194/gmd-10-709-2017>
- Tans, P. P., Fung, I. Y., & Takahashi, T. (1990). Observational Constraints on the global atmospheric CO₂ budget. *Science*, 247(4949), 1431–1438. <https://doi.org/10.1126/science.247.4949.1431>
- Thornton, P. E., Law, B. E., Gholz, H. L., Clark, K. L., Falge, E., Ellsworth, D. S., ... Sparks, J. P. (2002). Modeling and measuring the effects of disturbance history and climate on carbon and water budgets in evergreen needleleaf forests. *Agricultural and Forest Meteorology*, 113(1-4), 185–222. [https://doi.org/10.1016/S0168-1923\(02\)00108-9](https://doi.org/10.1016/S0168-1923(02)00108-9)
- Tian, H., Xu, X., Lu, C., Liu, M., Ren, W., Chen, G., ... Liu, J. (2011). Net exchanges of CO₂, CH₄, and N₂O between China's terrestrial ecosystems and the atmosphere and their contributions to global climate warming. *Journal of Geophysical Research*, 116, G02011. <https://doi.org/10.1029/2010JG001393>
- Tian, H., Chen, G., Zhang, C., Liu, M., Sun, G., Chappelka, A., ... Vance, E. (2012). Century-scale responses of ecosystem carbon storage and flux to multiple environmental changes in the southern United States. *Ecosystems*, 15(4), 674–694. <https://doi.org/10.1007/s10021-012-9539-x>

- Tucker, C., Pinzon, J., Brown, M., Slayback, D., Pak, E., Mahoney, R., ... El Saleous, N. (2005). An extended AVHRR 8-km NDVI dataset compatible with MODIS and SPOT vegetation NDVI data. *International Journal of Remote Sensing*, 26(20), 4485–4498. <https://doi.org/10.1080/01431160500168686>
- Urbanski, S., Barford, C., Wofsy, S., Kucharik, C., Pyle, E., Budney, J., ... Munger, J. W. (2007). Factors controlling CO₂ exchange on timescales from hourly to decadal at Harvard Forest. *Journal of Geophysical Research*, 112, G02020. <https://doi.org/10.1029/2006JG000293>
- van der Tol, C., Verhoef, W., & Rosema, A. (2009). A model for chlorophyll fluorescence and photosynthesis at leaf scale. *Agricultural and Forest Meteorology*, 149(1), 96–105. <https://doi.org/10.1016/j.agrformet.2008.07.007>
- van Dijk, A. I. J. M., Dolman, A. J., & Schulze, E.-D. (2005). Radiation, temperature, and leaf area explain ecosystem carbon fluxes in boreal and temperate European forests. *Global Biogeochemical Cycles*, 19, GB2029. <https://doi.org/10.1029/2004GB002417>
- Walther, S., Voigt, M., Thum, T., Gonsamo, A., Zhang, Y., Koehler, P., ... Guanter, L. (2015). Satellite chlorophyll fluorescence measurements reveal large-scale decoupling of photosynthesis and greenness dynamics in boreal evergreen forests. *Global Change Biology*, 22, 2979–2996. <https://doi.org/10.1111/gcb.13200>
- Wei, H., Chen, X., Xiao, G., Guenet, B., Vicca, S., & Shen, W. (2015). Are variations in heterotrophic soil respiration related to changes in substrate availability and microbial biomass carbon in the subtropical forests? *Scientific Reports*, 5, 18370. <https://doi.org/10.1038/srep18370>
- Wei, Y., Liu, S., Huntzinger, D. N., Michalak, A. M., Viovy, N., Post, W. M., ... Shi, X. (2014a). NACP MsTMIP: Global and North American Driver Data for Multi-Model Intercomparison. <https://doi.org/10.3334/ORNLDAAAC/1220>
- Wei, Y., Liu, S., Huntzinger, D. N., Michalak, A. M., Viovy, N., Post, W. M., ... Shi, X. (2014b). The North American Carbon Program Multi-scale Synthesis and Terrestrial Model Intercomparison Project—Part 2: Environmental driver data. *Geoscientific Model Development*, 7(6), 2875–2893. <https://doi.org/10.5194/gmd-7-2875-2014>
- Yang, H., Yang, X., Zhang, Y., Heskell, M. A., Lu, X., Munger, J. W., ... Tang, J. (2016). Chlorophyll fluorescence tracks seasonal variations of photosynthesis from leaf to canopy in a temperate forest. *Global Change Biology*, 23, 2874–2886. <https://doi.org/10.1111/gcb.13590>
- Yang, X., Tang, J., Mustard, J. F., Lee, J.-E., Rossini, M., Joiner, J., ... Richardson, A. D. (2015). Solar-induced chlorophyll fluorescence that correlates with canopy photosynthesis on diurnal and seasonal scales in a temperate deciduous forest. *Geophysical Research Letters*, 42, 2977–2987. <https://doi.org/10.1002/2015GL063201>
- Zeng, N., Mariotti, A., & Wetzell, P. (2005). Terrestrial mechanisms of interannual CO₂ variability. *Global Biogeochemical Cycles*, 19, GB1016. <https://doi.org/10.1029/2004GB002273>
- Zhang, Y., Xiao, X., Jin, C., Dong, J., Zhou, S., Wagle, P., ... Moore, B. III (2016). Consistency between Sun-induced chlorophyll fluorescence and gross primary production of vegetation in North America. *Remote Sensing of Environment*, 183, 154–169. <https://doi.org/10.1016/j.rse.2016.05.015>
- Zhu, Z., Bi, J., Pan, Y., Ganguly, S., Anav, A., Xu, L., ... Myneni, R. B. (2013). Global data sets of vegetation leaf area index (LAI)3g and fraction of photosynthetically active radiation (FPAR)3g derived from Global Inventory Modeling and Mapping Studies (GIMMS) normalized difference vegetation index (NDVI)3g for the period 1981 to 2011. *Remote Sensing*, 5(2), 927–948. <https://doi.org/10.3390/rs5020927>
- Zscheischler, J., Michalak, A. M., Schwalm, C., Mahecha, M. D., Huntzinger, D. N., Reichstein, M., ... Zeng, N. (2014). Impact of large-scale climate extremes on biospheric carbon fluxes: An intercomparison based on MsTMIP data. *Global Biogeochemical Cycles*, 28, 585–600. <https://doi.org/10.1002/2014GB004826>